Fitting quantum machine learning potentials to experimental free energy data: Predicting tautomer ratios in solution

Marcus Wieder* (0000-0003-2631-8415)[1*], **Josh Fass*** (0000-0003-3719-266X)[1,2], **John D. Chodera** (0000-0003-0542-119X)[1]

[*]contributed equally to this work; [1]Computational and Systems Biology Program, Sloan Kettering Institute, Memorial Sloan Kettering Cancer Center, New York, NY 10065, USA; [2]Tri-Institutional PhD Program in Computational Biology and Medicine, Weill Cornell Graduate School of Medical Sciences, New York, NY 10065, USA

***For correspondence:**
marcus.wieder@choderalab.org (MW)

Abstract The computation of tautomer rations of druglike molecules is enormously important in computer-aided drug discovery, as over a quarter of all approved drugs can populate multiple tautomeric species in solution. Unfortunately, accurate calculations of aqueous tautomer ratios—the degree to which these species must be penalized in order to correctly account for tautomers in modeling binding for computer-aided drug discovery—is surprisingly difficult. While quantum chemical approaches to computing aqueous tautomer ratios using continuum solvent models and rigid-rotor harmonic-oscillator thermochemistry are currently state of the art, these methods are still surprisingly inaccurate despite their enormous computational expense. Here, we show that a major source of this inaccuracy lies in the breakdown of the standard approach to accounting for quantum chemical thermochemistry using rigid rotor harmonic oscillator (RRHO) approximations, which are frustrated by the complex conformational landscape introduced by the migration of double bonds, creation of stereocenters, and introduction of multiple conformations separated by low energetic barriers induced by migration of a single proton. Using quantum machine learning (QML) methods that allow us to compute potential energies with quantum chemical accuracy at a fraction of the cost, we show how rigorous alchemical free energy calculations can be used to compute tautomer ratios in vacuum free from the limitations introduced by RRHO approximations. Furthermore, since the parameters of QML methods are tunable, we show how we can train these models to correct limitations in the underlying learned quantum chemical potential energy surface using free energies, enabling these methods to learn to generalize tautomer free energies across a broader range of predictions.

Introduction

The most common form of tautomerism, *prototropic tautomerism* describes the reversible structural isomerism involving the sequential processes of bond cleavage, skeletal bond migration and bond reformation in which a H^+ is transferred [1]. According to the IUPAC Gold Book, tautomers can be defined by the general equilibrium shown below in which X, Y, and Z are any of C, N, O, or S:

$$\mathrm{H-X-Y=Z} \xrightleftharpoons{\text{tautomerism}} \mathrm{X=Z-Y-H}$$

Numerous chemical groups can show prototropic tautomerism. Common examples include keto-enol (shown in Figure 2), amide/imidic acid, lactam/lactim, and amine/imine tautomerism [2].

Tautomerism influences many aspects of chemistry and biology

Tautomerism adds a level of mutability to the static picture of chemical compounds. How chemists think about and represent molecules is still largely influenced by the work of Kekulé and Lewis from the dawn of the 20th century [3]. The widespread usage of notating and representing chemical structure as undirected graphs with atoms as nodes and bonds as edges (and bond types annotated as edge attributes like single, double and triple bond) dominates the field of chemistry (with the notable exception of quantum chemistry) [4]. Tautomers make a satisfying description of chemical identity difficult in such a framework, since they can instantaneously change their double bond pattern and connectivity table if confronted with simple changes in environment conditions or exist as multiple structures with different connection table and bond pattern at the same time [5].

The change in the chemical structure between different tautomeric forms of a molecule is accompanied by changes in physico-chemical properties. By virtue of the movement of a single proton and the rearrangement of double bonds, tautomerism can significantly alter a molecule's polarity, hydrogen bonding pattern, its role in nucleophilic/electrophilic reactions, and a wide variety of physical properties such as partition coefficients, solubilities, and pKa [6, 7].

Tautomerism can also alter molecular recognition, making it an important consideration for supramolecular chemistry. To optimizing hydrogen bond patterns between a ligand and a binding site tautomerismn has to be considered. One of the most intriguing examples is the role that the tautomeric forms of the four building blocks of deoxynucleic acids played in the elucidation of biologically-relevant base pairings. The now well known Watson-Crick base pairing is only possible with guanine and cytosine in their amino (instead of imino) form and adenine and thymine in their lactam (instead of lactim) form. Watson and Crick struggled in their first attempts to get the tautomeric form of guanine right, delaying their work for a couple of weeks [2]. In the end, they concluded: "If it is assumed that the bases only occur in the most plausible tautomeric forms . . . only one specific pair of bases can bond together" [8]. The significance of this anecdote should not be underestimated. In a theoretical study of all synthetic, oral drugs approved and/or marketed since 1937, it has been found that 26% exist as an average of three tautomers [9]. While tautomerism remains an important phenomena in organic chemistry, it has not gained much appreciation in other scientific fields and there is little reason to doubt that such mistakes might repeat themselves in different settings [5].

The typical small energy difference between tautomers poses additional challenges for protein-ligand recognition. Local charged or polar groups in the protein binding pocket can shift the tautomer ratio and result in dominant tautomers in complex otherwise not present in solution [4]. For this reason the elucidation of the *dominant* tautomer in each environment is not enough — without the knowledge about the ratio (i.e. the free energy difference) between tautomeric forms in the corresponding phase a correct description of the experimental (i.e. macroscopic) binding affinity might not be possible. To illustrate this one might think about two extreme cases: one in which the tautomer free energy in solution is 10 kcal/mol and one in which it is 1.0 kcal/mol. It seems unlikely that the tautomer free energy difference of 10 kcal/mol will be compensated by the protein binding event (therefore one could ignore the unlikely *other* tautomer form), but a tautomer free energy difference of 1 kcal/mol could easily be compensated. Examples for this effect — changing tautomer ratios between environments — are numerous for vacuum and solvent phase. One example is the neutral 2-hydroxypyridine(2-HPY)/2-pyridone(2-PY) tautomer. The gas phase internal energy difference between the two tautomers is circa 0.7 kcal/mol in favor of the enol form (2-HPY), while in water

an internal energy difference of 2.8 kcal/mol was reported in favour of 2-PY. In cyclohexane, both tautomer coexist in comparable concentration while the 2-PY is dominant in solid state and polar solvents [10].

The example above assumed two tautomeric forms — if there were multiple tautomeric forms, each with small free energy differences, using a single dominant tautomer in solvent and complex may still represent only a minor fraction of the true equilibrium tautomer distribution.

The study of tautomer ratios requires sophisticated experimental and computational approaches

The experimental study of tautomer ratios is highly challenging [11]. The small free energy difference and low reaction barrier between tautomers—as well as their short interconversion time—can make it nearly impossible to study specific tautomers in isolation. Also, tautomer ratios can be highly sensitive to pH, temperature, salt concentration, solvent and environment [9]. The majority of available quantitative tautomer data is obtained from NMR and UV-vis spectroscopy, in combination with chemometric methods [5]. Recently, efforts have been made to collect some of the experimental data and curate these in publicly available databases, specifically Wahl and Sander [12] and Dhaked et al. [13].

In the absence of a reliable, cheap, and fast experimental protocol to characterize tautomeric ratios for molecules, there is a need for computational methods to fill the gap. And — even if such a method exists — predicting tautomer ratios of molecules that are not yet synthesized motivates the development of theoretical models. Computational methods themselves have a great need for defined tautomer ratios. Most computational methods use data structures in which bond types and/or hydrogen positions have to be assigned a priori and remain static during the calculation, introducing significant errors if an incorrect dominant tautomer is chosen [14]. This is true for a wide variety of methods including molecular dynamics/Monte Carlo simulations (and free energy calculations based on them), quantum chemical calculations (heat and energy of formation, proton affinities, dipole moments, ionization potentials (e.g. Civcir [15])), virtual screening [16], QS/PAR, docking, many molecular descriptors, and pKa/logD/logP calculations [9].

In the last 20 years, a multitude of different studies (see Nagy [17, 18] for a good overview) have been conducted using a wide variety of methods ranging from empirical (e.g. Milletti et al. [16]), force field based [19] to quantum chemical calculations [20] to investigate tautomer ratios in solution (or, more generally, proton transfer).

The third round of the Statistical Assessment of the Modeling of Proteins and Ligands (SAMPL2) challenge included the blind prediction of tautomer ratios and provided an interesting comparison between different computational methods [21]. Most of the 20 submissions were using implicit solvent models and ab initio or DFT methods to evaluate the energy differences [21]. Typically, such calculations use a thermodynamic cycle to assess the solution phase free energy (as shown in Figure 1). The Gibbs free energy is calculated in vacuum and the transfer free energy added using a continuum solvation model to obtain the free energy in solution. However, as stated in Martin [22], “In summary, although quantum chemical calculations provide much insight into the relative energies of tautomers, there appears to be no consensus on the optimal method”. For the 20 tautomer pairs investigated in the SAMPL2 challenge (this includes 13 tautomer pairs for which tautomer ratios were provided beforehand) the three best performing methods reported an RMSE of 2.0 [23], 2.5 [24] and 2.9 kcal/mol [25]. While these results are impressive it also shows that there is clearly room for improvement. And, maybe even more importantly, the SAMPL2 challenge showed the need for investigating a wider variety of tautomer transitions to draw general conclusions about best practice/methods for tautomer predictions [21]. The excellent review of Nagy concluded that tautomer relative free energies are sensitive to “the applied level of theory, the basis set used both in geometry optimization and [...] single point calculations, consideration of the thermal corrections [...] and the way of calculating the relative solvation free energy” [17]. We’d like to add “quality of 3D coordinates” to these issues and discuss them in the following.

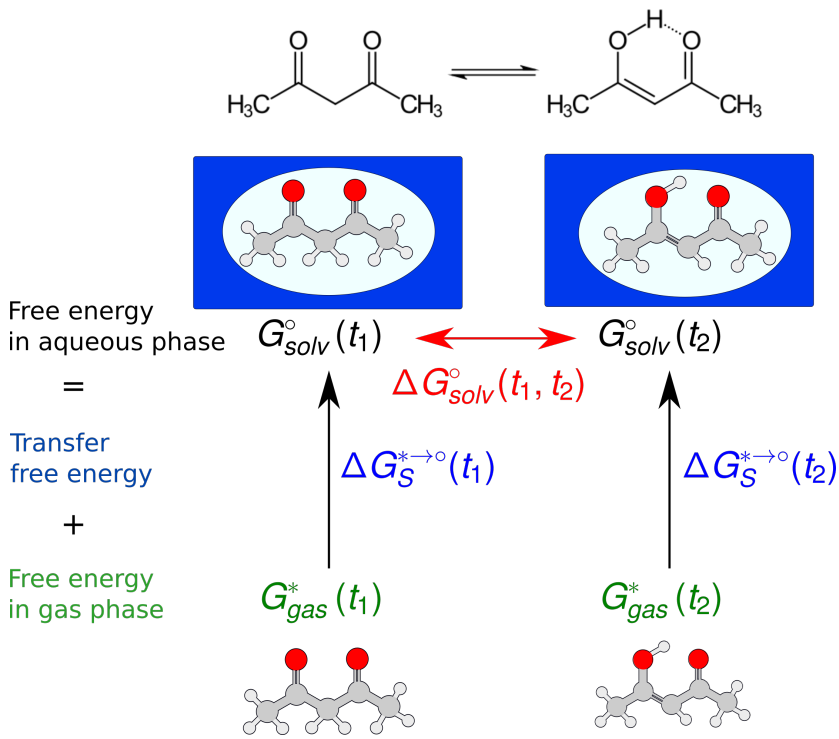

Figure 1. Solvation free energies are typically calculated using a thermodynamic cycle, independent of the level of theory that is used to obtain the individual terms. A typical quantum chemistry protocol calculates the free energy in aqueous phase (G°_{solv}) as the sum of the free energy in gas phase (G^{*}_{gas}; calculated using the ideal gas RRHO approximation) and the standard state transfer free free energy ($\Delta G^{*\rightarrow\circ}_{S}$; obtained using a continuum solvation model). The solvation free energy ΔG°_{solv} is then calculated as the difference between G°_{solv} for two tautomers.

Standard approaches to quantum chemical calculations of tautomer ratios introduce significant errors

Solvation free energy ΔG°_{solv} can be calculated from the standard-state Gibbs free energy in solution of the product and educt of the corresponding tautomer reaction. ΔG°_{solv} is computed as the difference in the free energies of both tautomer species, with the free energy of each tautomer in solution calculated as the sum of the gas-phase free energy $G^{*}_{gas,k}$ and the standard state solvation free energy $\Delta G^{*\rightarrow\circ}_{S,k}$ expressed as

$$G^{\circ}_{solv,k} = G^{*}_{gas,k} + \Delta G^{*\rightarrow\circ}_{S,k} \tag{1}$$

for a given conformation k and shown as a thermodynamic cycle in Figure 1.

The standard state gas phase free energy G^{*}_{gas} of conformation k at temperature T is defined as

$$G^{*}_{gas,k} = E_k + \epsilon_{ZPE,k} + G^{*}_{T,k} - RTlnD \tag{2}$$

with E_k as the electronic energy in the gas phase for a given conformation k, $\epsilon_{ZPE,k}$ the zero point energy (ZPE) correction, $G^{*}_{T,k}$ the thermal contribution to the Gibbs free energy for conformer k at temperature T and D the degeneracy of the ground electronic state in the standard state at 1 atm [26].

The standard-state Gibbs free energy is calculated using a quantum chemistry estimate for the electronic energy and, based on its potential energy surface, a statistical mechanics approximation to estimate its thermodynamic properties. While the accuracy of the electronic energy and the transfer free energy ΔG_S is dependent on the chosen method and can introduce significant errors in the following we want to concentrate on the approximations made by the thermochemical correction to obtain the gas phase free energy: the rigid rotor harmonic oscillator approximation and the use of single or multiple minimum conformation/s to generate a discret partition function.

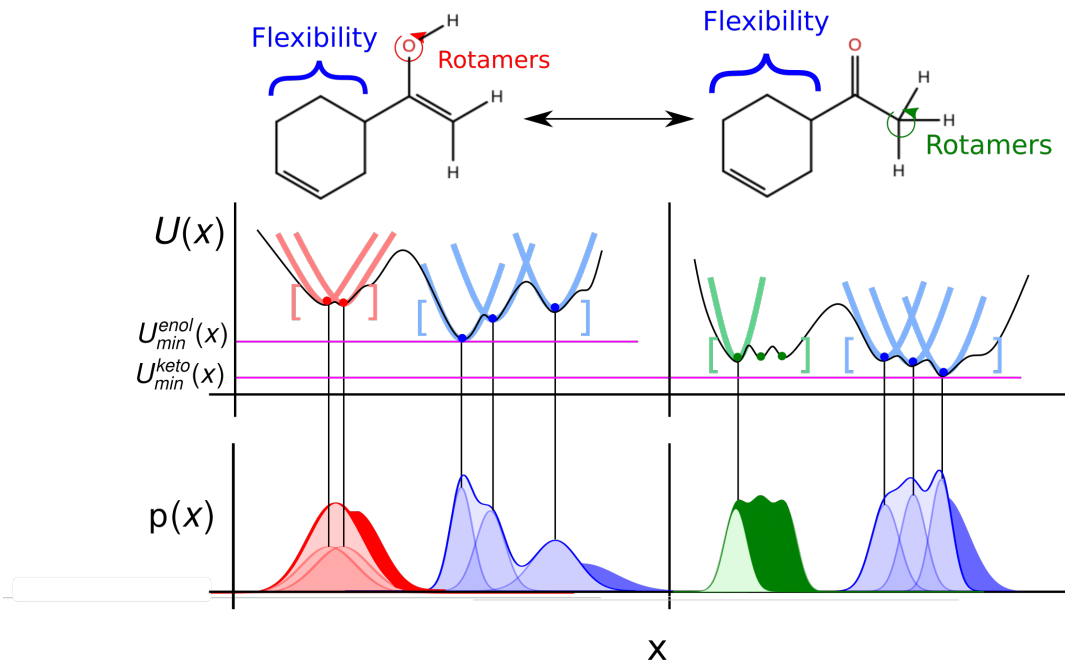

Figure 2. The rigid-rotor harmonic oscillator approach constructs a partition function using the curvature of the potential energy landscape at a minimum modelling all bonded terms as harmonic. The enol and keto form of a molecules (in the enol form: 1-(cyclohex-3-en-1-yl)ethen-1-ol) is shown and the main conformational degrees of freedom highlighted. The middle panel shows how the use of a local and harmonic approximation to the partition function can approximate the overall potential energy landscape, if all relevant minimum conformations are enumerated. The lower panel shows the probability density resulting from the harmonic approximations, with solid colored regions the difference between the true and approximated probability density resulting from anharmonicity and/or bonded terms that would better be modeled using a hindered/free rotor.

Rigid rotor harmonic oscillator can approximate the local configurational integral

A commonly used approach for the ZPE and thermal contributions is based on the ideal gas rigid rotor approximation (RRHO), assuming that the molecule is basically rigid and its internal motions comprise only vibrations of small amplitude where the potential energy surface can be approximated as harmonic around a local energy minimum. This assumption leads to an analytical approximation that describes the local configuration space around a single minimum based on the local curvature of the potential energy surface (Figure 2). The RRHO partition function Q_{RRHO} is assumed to be separable in the product of translational Q_{trans}, rotational Q_{rot}, and vibrational Q_{vib} terms. Using these approximations thermodynamic properties can be calculated using the molecule's geometry, frequencies/normal modes, and electronic state [27].

Errors are introduced because the harmonic oscillator approximation assumes that, for each normal mode, the potential energy associated with the molecule's distortion from the equilibrium geometry has a harmonic form. Especially low-frequency torsional modes would be more appropriately treated as hindered internal rotations at higher temperatures. This can lead to a significant underestimate of the configurational entropy, ignoring the contributions of multiple energy wells [28]. The correct treatment of such low-frequency modes in the analytical rotational entropy part of the RRHO partition function can add considerable computational cost, since the numerical solution requires the calculation of the full torsion potential (periodicity and barrier heights). Given that errors in the partition function are multiplicative and molecules may have several low-frequency torsional modes it is of interest to minimize their contribution to the final result [29].

Multiple local configurational integrals can be used to construct a discrete partition function

The free energy and all other standard thermodynamic properties of a system in a given thermodynamic ensemble are accessible through its partition function Q integrated over all possible conformations x [27]

$$Q = \int e^{-u(x)}\, dx \approx \sum_{k=1}^{N} q_k \tag{3}$$

where $u(x)$ denotes the reduced potential energy at coordinate set x. Given N local energy minima, the partition function can be approximated as a sum of N local integrals q_k [30]. The local partition function q_k restricted to energy well k can be written as

$$q_k = \int_k e^{-u(x)}\, dx \approx Q(k)_{RRHO} \tag{4}$$

with $Q(k)_{RRHO}$ as the RRHO partition function at the local minimum conformation k_{min}. The partition function Q can be approximated as a sum of contributions from the system's predominant low-energy conformations.

The standard state free energy G° of a molecule can then be calculated from the molar thermodynamic functions (in detail described in e.g. [27]) for each of the minimum conformations separately and combined as follows

$$G^\circ = -RT \ln\left(\sum_{k=1}^{N} e^{-G_k^\circ/RT}\right) \tag{5}$$

to obtain a weighted free energy k [26, 31]. The free energy obtained in equation 5 mitigates the shortcomings of the RRHO approach to model torsion with periodicity of 1 since — as long as the different minimas of the torsion are generated as conformations — these are included in the sum over all conformations.

Alchemical free energy calculations with machine learning potentials can compute true tautomer free energy differences, including all classical statistical mechanical effects

Limitations of the ideal gas RRHO approximation to the free energy and ZPE correction, challenges in enumeration of local minima, and the consistent treatment of internal/external rotational symmetry, as well as approximations in the continuum solvent model can lead to errors in the free energy that are difficult to detect and correct. The use of molecular dynamics simulations, explicit solvent molecules, and a rigorous classical treatment of nuclear motion to sample independent conformations from an equilibrium distribution can overcome the above mentioned challenges. To describe solvation free energies of tautomer pairs this would require computationally prohibitive QM/MM calculations in which the molecule of interest is treated quantum mechanically and the solute treated with molecular mechanics.

One of the most exciting developments in recent years has been the introduction of fast, efficient, accurate and transferable machine learning potentials (QML) (e.g. ANI [32], PhysNet [33], and SchNet [34]) to model organic molecules. QML potentials can be used to compute QM-based Hamiltonians and—given sufficient and appropriate training data—are able to reproduce electronic energies and forces without loss of accuracy but with orders of magnitude less computational cost than the QM methods they aim to reproduce. QML potentials have been successfully applied to molecular dynamics (MD) and Monte Carlo (MC) simulations [35]. Here, we present the application of a machine learning potential for the calculation of *alchemical free energies* for tautomer pairs in the gas phase.

We begin by investigating the accuracy of a current, state of the art approach to calculate tautomer ratios. We are using a popular DFT functional (B3LYP) and basis sets (aug-cc-pVTZ and 6-31G(d)) [36–40] for the calculation of the electronic energy and the continuum solvation model (SMD [41]) to model the transfer free energy. We are investigate its performance on a large set of diverse tautomer pairs spanning both different tautomer reactions, size and functional groups. We have selected a subset of 468 tautomer pairs from the publicly available *Tautobase* dataset [12] and performed quantum chemical geometry optimization, frequency calculation, single point energy, and thermochemistry calculations in gas and solvent phase using B3LYP/aug-cc-pVTZ and B3LYP/6-31G(d). This should significantly add to the canon of tautomer ratio studies.

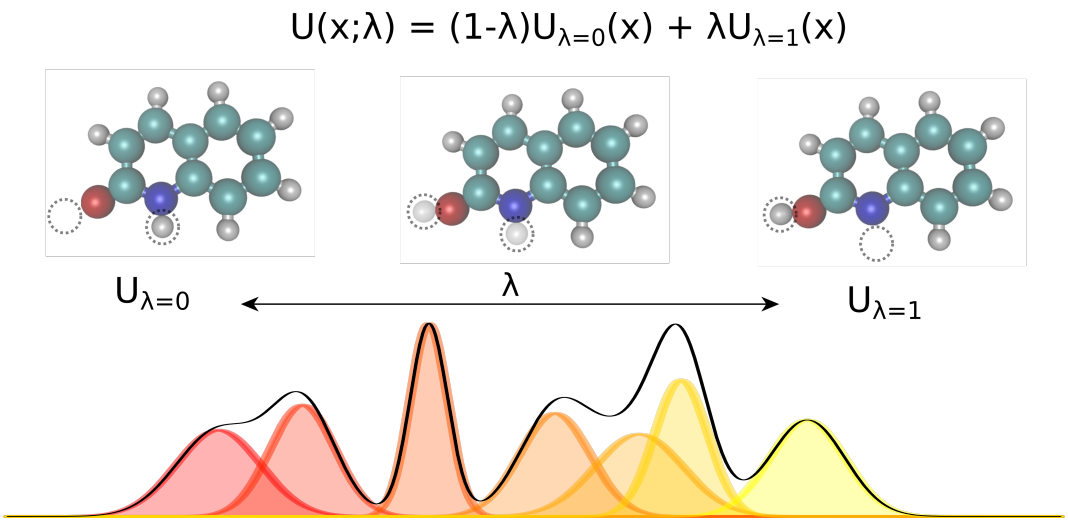

Figure 3. Alchemical free energy calculations with quantum machine learning (QML) potentials like ANI can rigorously compute free energy differences. Linearly interpolating between two potential energy functions using the alchemical parameter λ enables the sampling of bridging distributions between the physical endstates representing the two tautomers. Here, non interacting dummy atoms—indicated by the empty circle at each endstate—are included to facilitate this transformation. In this work, we present the application of this concept to calculate relative free energies of tautomer pairs in vacuum.

Furthermore we are investigating the effect of a more rigorous statistical mechanics treatment of the gas phase free energies. To analyse this we calculate gase phase free energy differences ΔG_{vac}^{calc} using (1) alchemical free energy calculations and (2) multiple minimum conformations in combination with the RRHO approximation (as used in the quantum chemistry approach). To enable a direct comparison between the two approaches we are using a QML potential for both approaches.

Since we are interested in solvation free energies we investigate the possibility to optimize the QML parmaters to include crucial solvent effects. The framework we have developed to perform alchemical free energy calculations for tautomer pairs enables us to obtain a relative free energy estimate that can be optimized with respect to the QML parameters. We are using a small training set of experimentally *solvation* free energies ΔG_{solv}^{exp} and importance sampling to obtain reweighted ΔG_{vac}^{calc} with the optimized parameters.

Here we report the first large scale investigation of tautomer ratios using quantum chemical calculations and machine learning potentials in combination with alchemical free energy calculations spanning a large chemical space and ΔG_{solv}^{exp} values.

Standard quantum chemistry methods predict tautomer ratios with a RMSE of 3.1 kcal/mol for a large set of tautomer pairs

Predicting free energy differences between tautomer pairs in solution ΔG^{calc}_{solv} is a challenging task since its success depends on a highly accurate estimate of both the intrinsic free energy difference between tautomer pairs as well as of their different contributions to the transfer free energy.

We calculated the free energy difference ΔG^{calc}_{solv} in solution for 468 tautomer pairs (460 if the basis set 6-31G(d) was used) and compared the results with the experimentally obtained values in Fig 4. The full results for all methods are given in Figure S.I.1. Three quantum chemistry approaches were used to calculate these values:

- **B3LYP/aug-cc-pVTZ/B3LYP/aug-cc-pVTZ/SMD**: Generating multiple conformations, optimizing with B3LYP/aug-cc-pVTZ in gas phase and solution phase (using the SMD continuum solvation model) and calculating ΔG^{calc}_{solv} as the sum of the gas phase free energy (evaluated on the in gas phase optimized conformation) and the difference between the single point energy in gas phase (gas phase conformations) and solvent (solvent phase conformation) calculated on the B3LYP/aug-cc-pVTZ level of theory. The individual free energies $\Delta G^{calc}_{solv,k}$ for conformation k are then Boltzmann averaged to obtain the final ΔG^{calc}_{solv}. Conformations were filtered based on heavy atom and heteroatom hydrogens root means square displacement of atoms (RMSD) (described in detail in the Methods section). This approach will be abbreviated with B3LYP/aug-cc-pVTZ/B3LYP/aug-cc-pVTZ/SMD in the following. The RMSE between ΔG^{exp}_{solv} and ΔG^{calc}_{solv} for the dataset is 3.4 [3.0;3.7] kcal/mol (the quantities [X;Y] denote a 95% confidence interval).
- **B3LYP/aug-cc-pVTZ/B3LYP/6-31G(d)/SMD** Generating multiple conformations, optimizing with B3LYP/aug-cc-pVTZ in gas phase and solution phase (using the SMD continuum solvation model) and calculating ΔG^{calc}_{solv} as the sum of the gas phase free energy (evaluated on the gas phase conformation) and the difference between the total energy in gas phase (evaluated on the gas phase conformation) and solvent phase (evaluated on the solvent phase conformation) on the B3LYP/6-31G(d) level of theory. The individual free energies $\Delta G^{calc}_{solv,k}$ for conformation k are then Boltzmann weithed to obtain the final ΔG^{calc}_{solv}. Conformations were filtered based on heavy atom and heteroatom hydrogens RMSD. The RMSE between ΔG^{exp}_{solv} and ΔG^{calc}_{solv} for the QM dataset is 3.1 [2.7;3.4] kcal/mol. This approach will be subsequently called B3LYP/aug-cc-pVTZ/B3LYP/6-31G(d)/SMD
- **B3LYP/aug-cc-pVTZ/SMD** Generating multiple conformations, optimizing with B3LYP/aug-cc-pVTZ in solution phase (using the SMD solvation model) and calculating ΔG^{calc}_{solv} directly as the difference between the RRHO free energy calculated in solution (and on the solution phase geometry). The individual $\Delta G^{calc}_{solv,k}$ for conformation k are then Boltzmann averaged to obtain the final ΔG^{calc}_{solv}. Conformations were filtered based on heavy atom and heteroatom hydrogens RMSD. The RMSE between ΔG^{exp}_{solv} and ΔG^{calc}_{solv} is 3.3 [3.0;3.7] kcal/mol. This approach will be subsequently called B3LYP/aug-cc-pVTZ/SMD.

The results for ΔG^{exp}_{solv} calculated with B3LYP/aug-cc-pVTZ/B3LYP/6-31G(d)/SMD are shown in Figure 4. The following discussion will concentrate on the results obtained with the best performing method (B3LYP/aug-cc-pVTZ/B3LYP/6-31G(d)/SMD). The results for all other methods are shown in the Supplementary Material Section.

The protocol used to obtain the results described above did not explicitly account for changes in symmetry (only changes in the point group were accounted for). The results including changes in the symmetry of the molecular graph are shown in Figure S.I.2 — the results are overall worse.

The best performing quantum chemistry method shows very good retrospective performance on the SAMPL2 tautomer set

Some of the tautomer pairs deposited in the Tautobase dataset were also part of the SAMPL2 challenge, specifically 6 out of 8 tautomer pairs of the obscure dataset (1A_1B, 2A_2B, 3A_3B, 4A_4B, 5A_5B, 6A_6B) and 8 out of 12 tautomer pairs of the explanatory dataset (7A_7B, 10B_10C, 10D_10C, 12D_12C, 14D_14C, 15A_15B, 15A_15C, 15B_15C) [21]. Comparing these molecules with the results of the SAMPL2 challenge—specifically with the results of the 4 participants with the best overall performance ([25], [42], [24], and

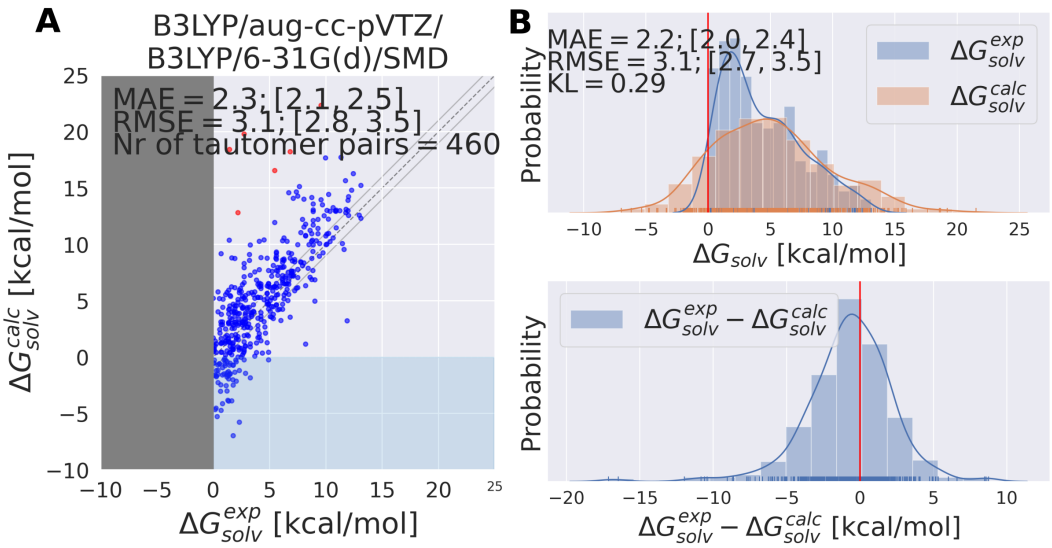

Figure 4. State of the art quantum chemistry calculations are able to calculate solvation free energy ΔG^{calc}_{solv} with a RMSE of 3.1 kcal/mol. The direction of the tautomer reaction is chosen so that the experimental solvation free energy ΔG^{exp}_{solv} is always positive. Panel **A** shows ΔG^{calc}_{solv} as the sum of the gas phase free energy and transfer free energy plotted against the experimental solvation free energy ΔG^{exp}_{solv}. B3LYP/aug-cc-pVTZ is used for the gas phase geometry optimization and single point energy calculation and the ideal gas RRHO approximation for the thermal corrections. The transfer free energy is calculated on B3LYP/aug-cc-pVTZ optimized geometries (for solvation phase with SMD as the continuum solvation model) using B3LYP/6-31G(d) and SMD. Values in quadrant II indicate calculations that assign the wrong dominant tautomer species (different sign of ΔG^{calc}_{solv} and ΔG^{exp}_{solv}). Red dots indicate tautomer pairs with more than 10 kcal/mol absolute error between ΔG^{calc}_{solv} and ΔG^{exp}_{solv}. These are separately shown in Table S.I.1. In Panel **B**, the top panel shows the kernel density estimate (KDE) and histogram of ΔG^{calc}_{solv} and ΔG^{exp}_{solv}. The red line indicates zero free energy difference (equipopulated free energies). In the lower panel the KDE of the difference between ΔG^{exp}_{solv} and ΔG^{calc}_{solv} is shown. MAE and RMSE are reported in units of kcal/mol. Quantities in brackets [X;Y] denote 95% confidence intervals. The Kullback-Leibler divergence (KL) was calculated using $KL(\Delta G^{exp}_{solv}||\Delta G^{calc}_{solv})$.

name	ΔG_{solv}^{exp}	ΔG_{solv}^{calc}	ΔG_{solv}^{calc}	ΔG_{solv}^{calc}	ΔG_{solv}^{calc}	ΔG_{solv}^{calc}
	[kcal/mol]	[kcal/mol]	[kcal/mol]	[kcal/mol]	[kcal/mol]	[kcal/mol]
		this work	[25][1]	[24][2]	[23][3]	[42][4]
1A_1B (982)	-4.8	-4.7	-4.0	-3.0	-7.7	-4.6
2A_2B	-6.1	-6.8	-5.7	-5.7	-9.7	-6.3
3A_3B (999)	-7.2	-8.4	-7.7	-6.7	-11.2	-7.7
4A_4B	-4.8	-0.4	0.5	0.8	-4.6	0.6
5A_5B (1614)	-4.8	-4.7	-3.9	-4.4	-6.2	-5.6
6A_6B (1005)	-9.3	-11.4	-7.6	-9.7	-11.2	-10.0
RMSE		1.3 [0.7,1.7]	1.4 [0.6,2.1]	1.5 [0.4,2.3]	2.8 [2.0,3.5]	1.3 [0.3,2.1]
7A_7B,(141)	6.6	4.9	5.3	6.5	5.1	5.5
10B_10C (1058)	-2.9	-5.3	1.7	0.0	-2.8	2.2
10D_10C (1059)	-1.2	-1.7	3.8	2.6	-0.6	5.0
12D_12C (1514)	-1.8	-2.1	3.3	3.1	-0.8	3.0
14D_14C (1072)	0.3	-1.6	1.9	0.8	0.2	4.0
15A_15B (504)	0.9	6.1	-3.0	3.6	0.0	0.9
15A_15C (505)	-1.2	0.7	-0.8	2.3	-1.9	1.4
15B_15C (506)	-2.2	-5.0	1.8	-1.2	-1.9	0.5
RMSE		2.5 [1.5,3.6]	3.6 [2.5,4.5]	2.9 [1.8,3.8]	0.8 [0.5,1.1]	3.8 [2.5,4.9]
Total RMSE		2.2 [1.4,2.9]	2.9 [2.0,3.6]	2.4 [1.6,3.1]	1.9 [1.2,2.6]	3.0 [1.9,4.0]

Table 1. Comparison between the results of this work and the SAMPL2 challenge. All values are given in kcal/mol. The calculations for Klamt and Diedenhofen [25] were performed with MP2+vib-CT-BP-TZVP, for Ribeiro et al. [24] with M06-2X/MG3S/M06-2X/6-31G(d)/SM8AD, Kast et al. [23] with MP2/aug-cc-pVDZ/EC-RISM/PSE-3, and Soteras et al. [42] with MP2/CBS+[CCSD-MP2/6-31+G(d)](d)/IEF-MST/HF/6-31G). On this subset the presented approach was the second best method based on the total RMSE. Bracketed quantities [X,y] denote 95% confidence intervals.

[23])—helps assess the quality of the chosen approach. Since all four mentioned participants employed different methods, we will briefly describe the best performing methods of these publications for which results are shown in Table 1. The references to the methods used below are not cited explicitly, these can be found in the publications cited at the beginning of the following paragraphs.

Klamt and Diedenhofen [25] used BP86/TZVP DFT geometry optimization in vacuum and the COSMO solvation model. Free energy in solvation was calculated from COSMO-BP86/TZVP solvation energies and MP2/QZVPP gas-phase energies. Thermal corrections (including ZPE) were obtained using BP86/TZVP ZPE.

Ribeiro et al. [24] calculated the free energy in solution as the sum of the gas-phase free energy and the transfer free energy. The gas phase free energy was calculated using M06-2X/MG3S level of theory and the molecular geometries optimized with the same method. The corresponding transfer free energy were computed at the M06-2X/6-31G(d) level of theory with the M06-2X/MG3S gas-phase geometries using the SM8, SM8AD, and SMD continuum solvation models (Table 1 shows only the results with SM8AD, which performed best).

Kast et al. [23] optimized geometries in gas and solution phase (using the polarizable continuum solvation model PCM) using B3LYP/6-311++G(d,p). Energies were calculated with EC-RISM-MP2/aug-cc-pVDZ on the optimized geometries in the corresponding phase. The Lennard-Jones parameters of the general Amber force field (GAFF) were used.

Soteras et al. [42] used the IEF-MST solvation model parameterized for HF/6-31G(G) to obtain transfer free energy values. Gas phase free energy differences were obtained by MP2 basis set extrapolation using the aug-cc-pVTZ basis set at MP2/6-31+G(d) optimized geometries. Correlation effects were computed from the CCSD-MP2/6-31+G(d) energy difference [43].

The approach used in this work (B3LYP/aug-cc-pVTZ/B3LYP/6-31G(d)/SMD) performs well compared to the four approaches described above. For the total set of investigated tautomer pairs our approach has a RMSE of 2.2 [1.4,2.9] kcal/mol, making it the second best performing approach only outperformed by Kast

et al. [23].

Interestingly to note is the difference in RMSE between the explanatory and blind dataset. Approaches that perform well on the blind data set are performing worse on the explanatory set and vice versa. This is to a lesser extent also true for our chosen approach—B3LYP/aug-cc-pVTZ/B3LYP/6-31G(d)/SMD performs worse for the explanatory tautomer set (RMSE of 2.5 [1.5,3.6] kcal/mol) than on the blind tautomer set (RMSE of 1.3 [0.7,1.7]), but in comparison with the other four approaches, it is consistently the second best approach.

Interesting to note are the three tautomer reactions 15A_15B, 15A_15C and 15B_15C from the explanatory data set. The absolute error for B3LYP/aug-cc-pVTZ/B3LYP/6-31G(d)/SMD are 5.24, 1.9, 2.8 kcal/mol. It appears that the used approach has difficulty to model 15B correctly, showing larger than average absolute errors whenever 15B is part of the tautomer reaction. Most likely the hydroxyl group in 15B is critically positioned and sensitive to partial solvent shielding by the phenyl ring, something that has been observed before [23].

The discrepancy between the different approaches (ours included) for the tautomer set show that it seems highly difficult to propose a single method for different tautomer pairs that performs consistently with a RMSE below 2.0 kcal/mol. This issue is made substantially worse by the many different ways methods can be used/combined and errors can be propagated/compensated during ΔG_{solv}^{calc} calculations. While we believe that a RMSE of 3.1 kcal/mol is a good value for the chosen approach, especially when compared to the results of the SAMPL2 challenge, it is by far not a satisfying result. The accuracy, compared to the cost of the approach, is not justifiable and there is still a dire need for more accurate and cheaper methods to obtain ΔG_{solv}^{calc}.

The molecules with the highest absolute error between the calculated and experimental tautomer free energies in solution have common substructures

5 out of the 6 molecules with highest absolute error between experimental ΔG_{solv}^{exp} and calculated solvation free energy ΔG_{solv}^{calc} (above 10 kcal/mol) have common scaffolds (values and molecules shown in the Supplementary Material Table S.I.1). molDWRow_1668, 1669, 1670 are all based on 5-iminopyrrolidin-2-one with either nitrogen, oxygen or sulfur on position 4 of the ring. molDWRow_1559 and molDWRow_853 both have methoxyethylpiperidine as a common substructure.

For the three analogues based on 5-iminopyrrolidin-2-one we want to note that the experimental values are estimated results based on a three-way tautomeric reaction [44]. While this might point to the unreliability of ΔG_{solv}^{exp}, we can not draw any definitive conclusions here without repeating the underlying experiment.

Including multiple minimum conformations seems to have little effect on the accuracy of solvation free energies

The three approaches described above (B3LYP/aug-cc-pVTZ/B3LYP/6-31G(d)/SMD, B3LYP/aug-cc-pVTZ/B3LYP/aug-cc-pVTZ/SMD and B3LYP/aug-cc-pVTZ/SMD) consider multiple conformations to obtain the solvation free energy ΔG_{solv}^{calc}. Obtaining the global minimum conformation is an important and well established task in quantum chemistry calculations. Figure 4 shows the free energy difference between the highest and lowest energy minimum conformation for the molecules from the dataset generated with B3LYP/aug-cc-pVTZ/B3LYP/6-31G(d)/SMD. While the majority of the molecules have only a single minimum conformation, for molecules with multiple minima the difference in the vacuum free energy emphasises the need and justifies the cost for a global minimum conformation search.

While the scientific community agrees on the importance of the global minimum for property calculations, the importance of considering multiple conformations for solvation free energy calculations has not been well established (e.g. [45]). The additional cost of frequency calculations (especially if an analytical Hessian is not available) on conformations other than the lowest energy one adds substantially to the overall cost of these calculations. If a single, minimum energy conformation is sufficient to obtain a good estimate for the vacuum free energy a lot of computational time could be saved.

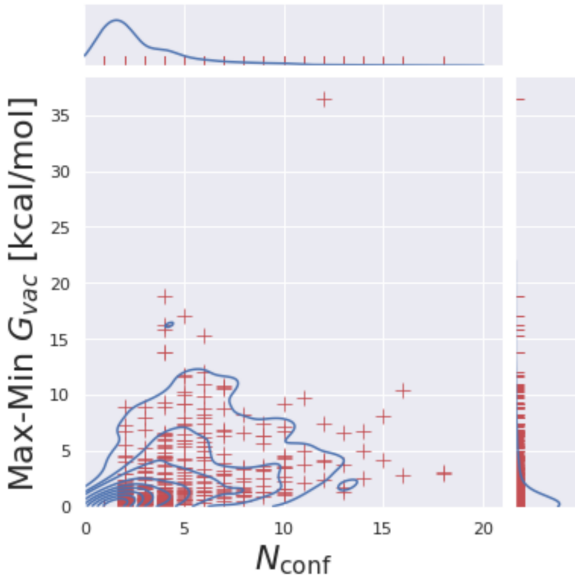

Figure 5. Computed solvation free energies are highly sensitive to the selected minimum conformation. For each molecule, the number of minima N_{conf} is plotted against the difference between the corresponding highest and lowest obtained free energy value. The majority of molecules have only a single minimum; molecules with multiple minima show substantial free energy differences between the minimum conformations highlighting the need for a global minimum search.

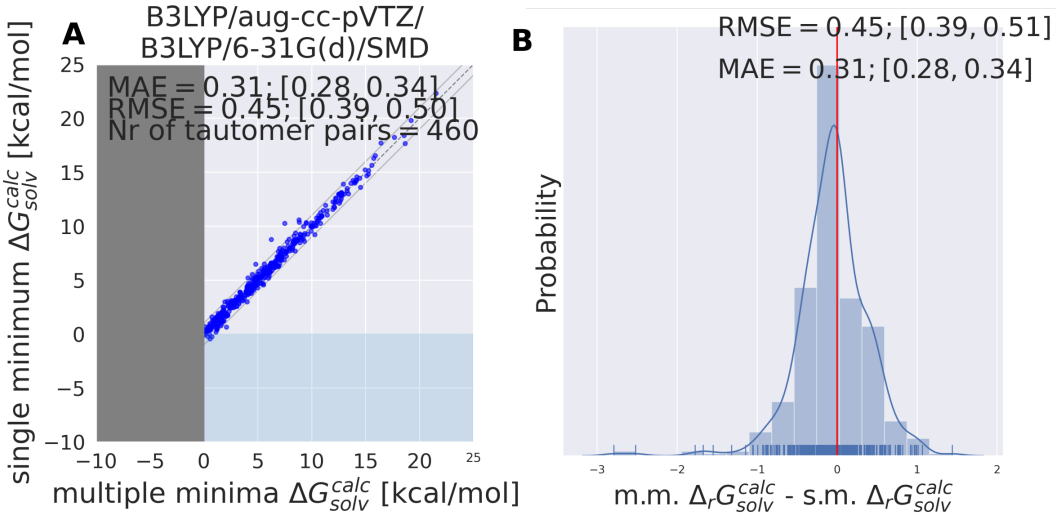

Figure 6. A single, global minimum conformation can be used to calculate solvation free energy differences without loss of accuracy. These results are based on the calculations with B3LYP/aug-cc-pVTZ/B3LYP/6-31G(d)/SMD. **A** shows the solvation free energy ΔG^{calc}_{solv} obtained with multiple minima (m.m.) plotted against the global, single minimum (s.m.) solvation free energy ΔG^{calc}_{solv}. **B** shows the KDE and histogram of the difference between s.m. ΔG^{calc}_{solv} and m.m. ΔG^{calc}_{solv}. The comparison indicates that there is little benefit using multiple minimum structures over a single, global minimum considering the high costs of the former.

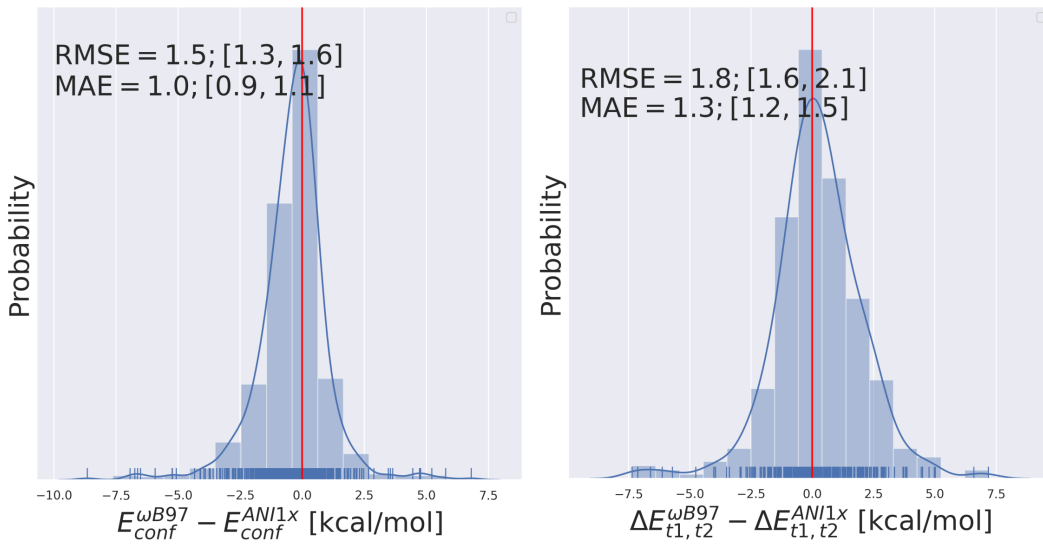

Figure 7. Despite not being trained on tautomers, the quantum machine learning potential ANI1x can compute single point energies of tautomers with high accuracy and similar RMSE as was previously reported for the training set in Smith et al. [32]. The difference between ANI1x and *omega* B97x/6-31G(d) (the quantum chemical method ANI1x was trained on) for single point energy calculations and single point energy differences of tautomer pairs are shown. 21 molecules for which the energy minimization failed were excluded from the analysis.

Figure 6 shows the results for the solvation free energies using the Boltzmann average over multiple minimum conformations plotted against the single global minimum conformation. The results indicate that using multiple minimum conformations does not significantly change the final result compared to using a single, global minimum structure. Only 12 tautomer pairs show an absolute error larger than 1 kcal/mol in ΔG_{solv}^{calc} between the two approaches. Much more relevant than including multiple conformations is locating the global minimum conformation (as clearly shown by Figure 5).

The quantum machine learning (QML) potential ANI1x can reproduce single-point energy differences between tautomers with high accuracy

The ANI family of machine learning potentials [32] were trained on a large dataset that spans conformational and configurational space and has shown astonishing accuracy and transferability in the prediction of molecular total energies. But ANI was not trained on tautomer species of molecules making an investigation in potential modelling errors of the neural net potential necessary.

To approach this question we calculated molecular total energies E with ANI1x and ω B97X/6-31G(d) on molecular conformations optimized with ω B97X/6-31G(d) for all tautomers in investigation. The difference between the total energies for a single tautomer (i.e. $(E_{conf}^{\omega B97x} - E_{conf}^{ANIx})$ and for tautomer pairs (i.e. $(E_{conf-t2}^{\omega B97x} - E_{conf-t1}^{\omega B97x}) - (E_{conf-t2}^{ANIx} - E_{conf-t1}^{ANIx})$) are shown in Figure 7. Tautomer pairs were excluded if one of them failed to converge to a minimum conformation during the optimization resulting in the removal of 21 tautomer pairs.

Single point energy calculations were performed using ANI1x with a RMSE of 1.5 [1.3,1.6] kcal/mol and a MAE of 1.0 [0.9,1.1] kcal/mol. 11.6 % (81/696) of single point energy calculations had a difference greater than 2 kcal/mol to the reference QM level of theory.

The difference between two single point energy calculations with ANI1x and its reference QM level of theory for the tautomer pairs had a slightly higher RMSE of 1.8 [1.6,2.1] kcal/mol and a MAE of 1.3 [1.2,1.5] kcal/mol. 22.1% (77/348) of tautomer pairs had a difference greater than 2 kcal/mol to the reference QM level of theory. There seems to be a small quantity of error compensation—a MAE of 1.3 [1.2,1.5] kcal/mol is in accordance with the expected error propagation for uncorrelated measurements.

Alchemical free energy calculations with quantum machine learning potentials can rigorously capture classical statistical mechanical effects in relative free energy calculations of tautomers

Alchemical free energy calculations were performed for 354 tautomer pairs using 11 alchemical intermediate λ states in vacuum.

In the following, we will compare the relative free energies obtained using alchemical free energy calculations with the multiple minima, RRHO approximation using the same potential energy function (ANI1ccx) to assess potential errors in the thermochemistry corrections. We will also show how a small number of experimental solvation free energy differences between tautomer pairs can be used to incorporate crucial solvent effects and recover solvation free energies by importance weighting and QML parameter optimization from alchemical vacuum free energy calculations.

RRHO ANI1ccx calculations show significant deviations from the alchemical free energy calculations

In the limit of infinite sampling alchemical free energy calculations approach the exact free energy difference. Alchemical free energy calculations can be used to quantify the error that a discrete partition function in the form of multiple minimum conformations and harmonic treatment of all bonded terms (including torsions and internal rotators) introduce—if the same electronic energy function is used for both calculations.

Since the simulation time of the individual lambda states for the alchemical free energy calculations were relatively short (200 ps) we ran multiple (5) experiments with randomly seeded starting conformations and velocities to detect systems for which the simulation time was clearly insufficient. In the following we will only use systems that had a standard deviation of less than 0.3 kcal/mol for the 5 independent relative free energy calculations. Applying this filter resulted in the removal of 65 tautomer pairs whose alchemical free energy calculations had not converged.

Results shown in Figure 8 for one of the 5 independent calculations indicate the average error that every relative free energy calculation based on the RRHO approximation introduces, regardless of the accuracy of the actual potential to model electronic energies. The mean absolute error of 0.9 kcal/mol should not be underestimated. Results shown in Table 1 would be significantly improved if an error of 0.9 kcal/mol could be compensated by running a protocol that samples the relevant conformational degrees of freedom to obtain an exact partition function.

For 12 (out of 289) tautomer pairs the multiple minima RRHO approximation introduces errors of more than 3 kcal/mol (molecules are shown in Figure 9). Most molecules shown have high conformational degrees of freedom and it seems unlikely that a naive conformational enumeration (like we used with a conformer generator) will detect all of them – this might contributed to the observed error. That is certainly true for molDWRow_113, 116, 565, 554, 403, 1674.

QML potentials can be optimized to reproduce experimental solvation free energy differences

The aim of this section is to show that we can use optimized QML parameters to include solvent effects and perform importance weighting from vacuum simulations. The term *free energy difference in vacuum* ΔG^{calc}_{vac} is still used here, even though we aim to model solvation free energies ΔG^{calc}_{solv}.

Since the alchemical free energy calculations were performed in vacuum, a comparison with the experimental solvation free energies ΔG^{exp}_{solv} showed a high RMSE of 6.4 [5.9,6.8] kcal/mol, as expected from the well-known impact of solvation effects on tautomer ratios [46].

Defining a loss function L as the mean squared error (MSE) between the calculated $\Delta G^{calc}_{vac}(\theta)$ and experimental ΔG^{exp}_{solv} free energy differences it is possible to minimize the loss with respect to the neural net parameters θ defining the ANI potential.

Using importance weighting, a new free energy estimate can be calculated with the optimized QML parameters (θ^*) using the modified potential energy function without resampling the equilibrium distributions.

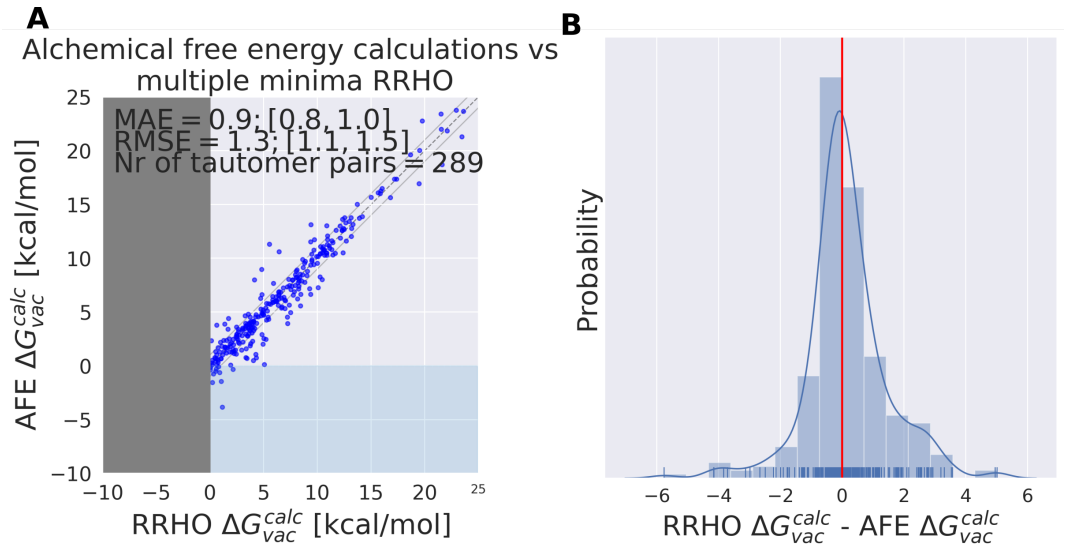

Figure 8. Independent of the level of theory, thermochemistry corrections introduce an average absolute error of 0.9 kcal/mol. ANI1ccx is used for the calculation of free energy differences ΔG^{calc}_{vac} in vacuum using alchemical free energy (AFE) calculations and single point energy calculations on multiple minimum conformations and thermochemistry corrections based on the RRHO approximation (RRHO). Results are shown for a single **A** shows a scatter plot between the two approaches and **B** the KDE and histogram of the difference between the two approaches. Error bars are shown in red on the alchemical free energy estimates, these were obtained from the MBAR estimate of the relative free energy.

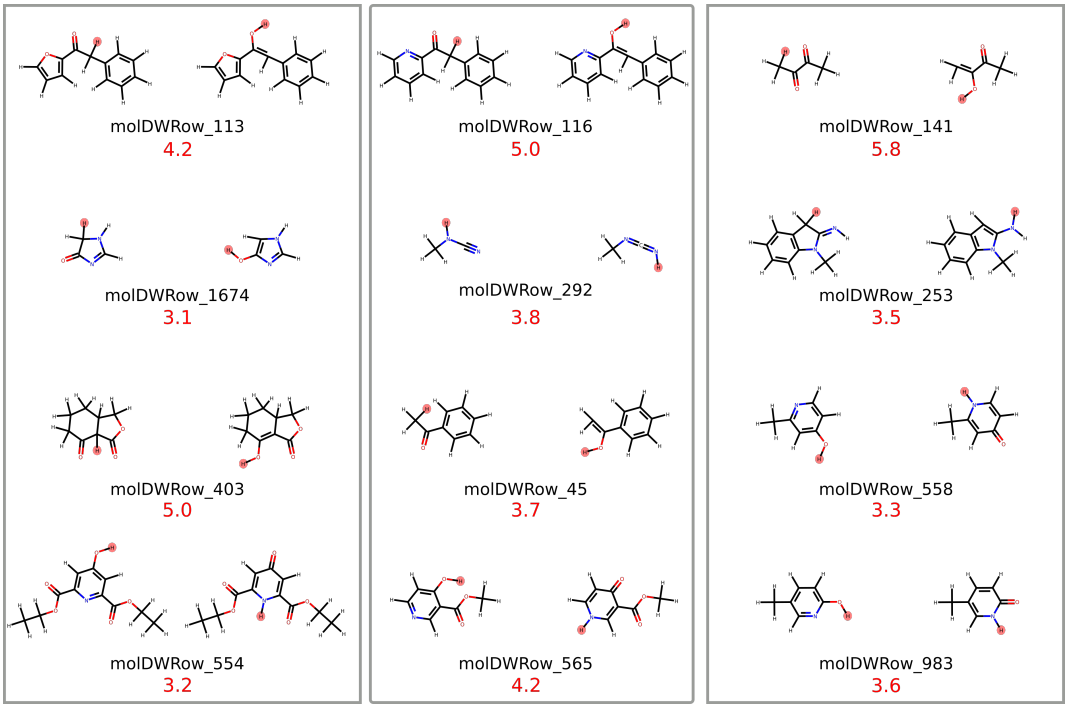

Figure 9. Molecules for which the RRHO approximation introduces an error of more than 3 kcal/mol are shown. Absolute error is shown in red (value in kcal/mol) The hydrogen that changes position is highlighted in red.

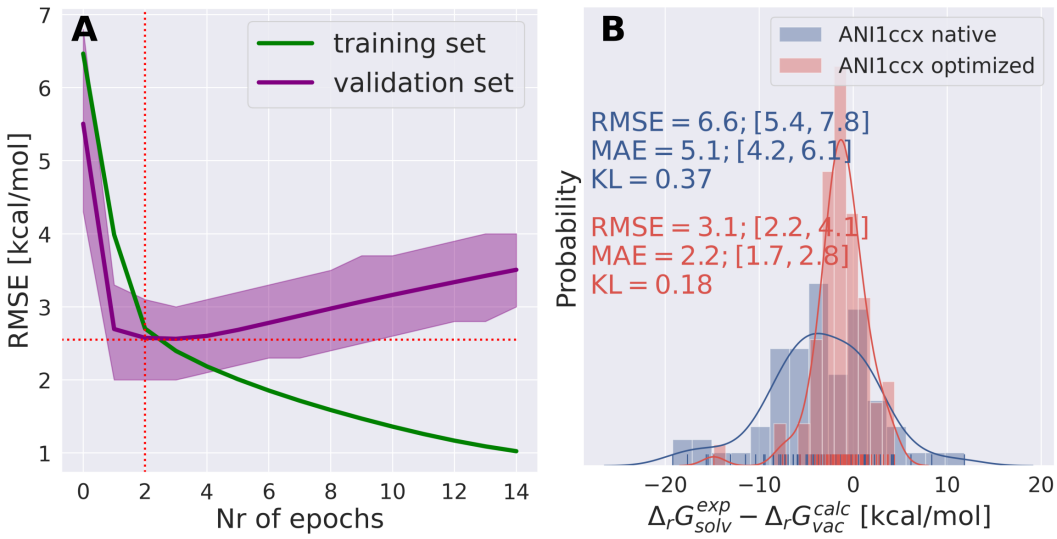

Figure 10. Optimizing QML parameters on a set of experimentally obtained solvation free energies ΔG^{exp}_{solv} enables ANI1ccx to include crucial solvation effects and good estimates for solvation free energies can be obtained by importance weighting from vacuum simulations using the improved QML parameters. A shows the training (green) and validation (purple) set performance (RMSE) as a function of epochs. Validation set performance was plotted with a bootstrapped 95% confidence interval. The best performing parameter set (evaluated on the validation set – indicated as the intersection between the two red dotted lines) was selected to compute the RMSE on the test set. Figure B shows the distribution of ΔG^{exp}_{solv} - ΔG^{calc}_{vac} for the tautomer test set (71 tautomer pairs) with the native ANI1ccx (θ) and the optimization parameter set (θ^*). The Kullback-Leibler divergence (KL) was calculated using $KL(\Delta G^{exp}_{solv}||\Delta G(\theta)^{calc}_{vac})$ for the native ANI1ccx and $KL(\Delta G^{exp}_{solv}||\Delta G(\theta^*)^{calc}_{vac})$ for the optimized parameter set.

Hereby, the accuracy of this estimate depends on the variability of the importance weights — the equilibrium distribution defined by the optimized QML parameters need to be fairly similar to work well (e.g. [47]). The used protocol is described in more details in the Methods section.

Figure 10 shows the obtained free energy estimates with the optimized QML parameters. The best performing QML parameters on the validation tautomer set were obtained after just two epochs of optimization (each including a single parameter optimization update per tautomer pair). Using validation-based early stopping the optimized QML parameters were used to calculate free energy differences in vacuum ΔG^{calc}_{vac} on an independent test set (71 tautomer pairs) show in Figure 10 B. The RMSE on the test set after optimization was decreased from 6.6 [5.4,7.8] kcal/mol to 3.1 [2.2,.8] kcal/mol, comparable to the performance of B3LYP/aug-cc-pVTZ/B3LYP/6-31G(d)/SMD.

Figure 10 B shows the distribution of ΔG^{exp}_{solv} - ΔG^{calc}_{vac}. The Kullback-Leibler divergence (KL) was calculated using $KL(\Delta G^{exp}_{solv}||\Delta G(\theta)^{calc}_{vac})$ for the native ANI1ccx and $KL(\Delta G^{exp}_{solv}||\Delta G(\theta^*)^{calc}_{vac})$ for the optimized parameter set. The KL value for $KL(\Delta G^{exp}_{solv}||\Delta G(\theta^*)^{calc}_{vac})$ shows that overall the optimized parameter set is able to reproduce the distribution of the experimental solvation free energies closely.

These results highlight the incredible potential of differentiable energies w.r.t input parameters, making the powerful optimization of the parameters easily accessible.

Discussion & Conclusion

In this work we use a state of the art density functional theory protocol and continuum solvation model to calculate tautomer ratios for 460 tautomer pairs using three different approaches to model the solvent contributions. The best performing method uses B3LYP/aug-cc-pVTZ and the rigid rotor harmonic oscillator approximation for the gas phase free energies (calculated on B3LYP/aug-cc-pVTZ optimized geometries). The transfer free energy was calculated using B3LYP/6-31G(d)/SMD on geometries optimized in their respective phase (with B3LYP/aug-cc-pVTZ). This approach performs with a RMSE of 3.1 kcal/mol.

One possible source of error — independent of the method used to calculate the electronic energy and

model the continuum electrostatics — are the thermochemical corrections used to obtain the standard state free energy. Typically, a analytical expression for the partition function is used that is based on the rigid rotor harmonic oscillator approximation. To obtain rigorous free energy estimates we implemented a relative alchemical free energy workflow using the ANI family of neural net (QML) potentials [32]. The method was implemented as a python package and is available here: https://github.com/choderalab/neutromeratio.

Using the same potential for the calculations based on the RRHO and performing alchemical relative free energy calculations we show that the RRHO approximation introduces a mean absolute error of circa 1 kcal/mol on the investigated tautomer data set. These errors can be attributed to anharmonicity in bonded terms, difficulties to enumerate all relevant minimum conformations, inconsistencies in combining shallow local energy wells as well as the inconsistent treatment of internal and external symmetry numbers.

The calculated alchemical free energies obtained using the methods implemented in the '"Neutromeratio"' package can be optimized with respect to the parameters of the QML potential. Using a small set of experimental solvation free energies we were able to show that we can significantly improve the accuracy of the calculated free energies on an independent test set.

What should be noted here: the experimental values are solvation free energies, while we calculate vacuum free energies. The optimization routine on the experimental solvation free energies adds crucial solvent effects to the accurate description of the vacuum potential energy. The ANI family of QML and comparable QML potentials have opened the possibility to investigate tautomer ratios using relative free energy calculations without prohibitive expensive MM/QM schemes.

Obtaining accurate free energy differences between tautomer pairs in solvent remains an elusive task. The sublet changes and typically small difference in internal energies between tautomer pairs require an accurate description of electronic structures. Furthermore, solvent effects have a substantial effect on tautomer ratios; consequently, a proper descriptor of solvation is essential. The change in double bond pattern typically also induce a change in the conformational degrees of freedom and, related, in the conformation and rotational entropy. But — despite all of these challenges — we remain optimistic that further developments in fast and accurate neural net potentials will enable improved and more robust protocols to use relative free energy calculations to address these issues.

Code and data availability

- Input files, results and setup scripts: https://github.com/choderalab/neutromeratio

Author Contributions

Conceptualization: JDC, JF, and MW; Methodology: JDC, JF, and MW; Software: JF, and MW; Investigation: JF, and MW; Writing–Original Draft: JDC, JF, and MW; Writing–Review&Editing: JDC, JF, and MW; Funding Acquisition: JDC and MW; Resources: JDC and MW; Supervision: JDC and MW.

Acknowledgments

MW, JF and JDC are grateful for discussions from the Tautomer Consortium, specifically Paul Czodrowski, Brian Radak, Woody Sherman, David Mobley, Christopher Bayly and Stefan Kast as well as input from Adrian Roitberg and Olexandr Isayev. This work was only possible through the time and effort Thomas Sander and Oya Wahl invested in curating the open tautomer database (Tautobase). Further, MW is grateful for the support of Thierry Langer, who donated significant computational resources to perform much of the calculations/simulations and Oliver Wieder, for helpful discussions.

Funding

JF acknowledges support from NSF CHE-1738979 and the Sloan Kettering Institute. MW acknowledges support from a FWF Erwin Schrödinger Postdoctoral Fellowship J 4245-N28. JDC acknowledges support from NIH grant P30 CA008748, NIH grant R01 GM121505, NIH grant R01 GM132386, and the Sloan Kettering Institute.

Disclosures

JDC is a current member of the Scientific Advisory Board of OpenEye Scientific Software and a consultant to Foresite Laboratories. The Chodera laboratory receives or has received funding from multiple sources, including the National Institutes of Health, the National Science Foundation, the Parker Institute for Cancer Immunotherapy, Relay Therapeutics, Entasis Therapeutics, Silicon Therapeutics, EMD Serono (Merck KGaA), AstraZeneca, Vir Biotechnology, Bayer, XtalPi, Foresite Laboratories, the Molecular Sciences Software Institute, the Starr Cancer Consortium, the Open Force Field Consortium, Cycle for Survival, a Louis V. Gerstner Young Investigator Award, and the Sloan Kettering Institute. A complete funding history for the Chodera lab can be found at http://choderalab.org/funding

References

[1] **Kapetanović I**. Drug Discovery and Development: Present and Future. IntechOpen; 2011.

[2] **Bax B**, Chung CW, Edge C, Getting the chemistry right: protonation, tautomers and the importance of H atoms in biological chemistry; 2017.

[3] **Lewis GN**, THE ATOM AND THE MOLECULE; 1916.

[4] **Sayle RA**, So you think you understand tautomerism?; 2010.

[5] **Taylor PJ**, van der Zwan G, Antonov L, Tautomerism: Introduction, History, and Recent Developments in Experimental and Theoretical Methods; 2013.

[6] **Sitzmann M**, Ihlenfeldt WD, Nicklaus MC, Tautomerism in large databases; 2010.

[7] **Katritzky AR**, Dennis Hall C, El-Gendy BEDM, Draghici B, Tautomerism in drug discovery; 2010.

[8] **Watson JD**, Crick FHC, THE STRUCTURE OF DNA; 1953.

[9] **Martin YC**, Let's not forget tautomers; 2009.

[10] **Hejazi S**, Osman O, Alyoubi A, Aziz S, Hilal R. The Thermodynamic and Kinetic Properties of 2-Hydroxypyridine/2-Pyridone Tautomerization: A Theoretical and Computational Revisit. International Journal of Molecular Sciences. 2016; 17(11):1893. http://www.ncbi.nlm.nih.gov/pubmed/27854244{%}250Ahttp://www.mdpi.com/1422-0067/17/11/1893, doi: 10.3390/ijms17111893.

[11] **Taylor PJ**, Antonov L, "Triage" for Tautomers: The Choice between Experiment and Computation; 2016.

[12] **Wahl O**, Sander T, Tautobase : An Open Tautomer Database; 2020.

[13] **Dhaked DK**, Guasch L, Nicklaus MC, Tautomer Database: A Comprehensive Resource for Tautomerism Analyses; 2020.

[14] **Pospisil P**, Ballmer P, Scapozza L, Folkers G. Tautomerism in Computer-Aided Drug Design. J Recept Signal Transduction. 2003 Jan; 23(4):361–371.

[15] **Civcir PÜ**, A theoretical study of tautomerism of cytosine, thymine, uracil and their 1-methyl analogues in the gas and aqueous phases using AM1 and PM3; 2000.

[16] **Milletti F**, Storchi L, Sforna G, Cross S, Cruciani G. Tautomer Enumeration and Stability Prediction for Virtual Screening on Large Chemical Databases. J Chem Inf Model. 2009 Jan; 49(1):68–75.

[17] **Nagy P**, Theoretical Calculations on the Conformational/Tautomeric Equilibria for Small Molecules in Solution; 2014.

[18] **Nagy PI**, Theoretical Consideration of In-Solution Tautomeric Equilibria in Relation to Drug Design; 2016.

[19] **Huang J**, Meuwly M, Force Field Treatment of Proton and Hydrogen Transfer in Molecular Systems; 2013.

[20] **Fabian WMF**, Quantum Chemical Calculation of Tautomeric Equilibria; 2013.

[21] **Geballe MT**, Geoffrey Skillman A, Nicholls A, Peter Guthrie J, Taylor PJ, The SAMPL2 blind prediction challenge: introduction and overview; 2010.

[22] **Martin YC**. Overview of the perspectives devoted to tautomerism in molecular design. J Comput Aided Mol Des. 2010 Jun; 24(6-7):473–474.

[23] **Kast SM**, Heil J, Güssregen S, Friedemann Schmidt K, Prediction of tautomer ratios by embedded-cluster integral equation theory; 2010.

[24] **Ribeiro RF**, Marenich AV, Cramer CJ, Truhlar DG. Prediction of SAMPL2 aqueous solvation free energies and tautomeric ratios using the SM8, SM8AD, and SMD solvation models. J Comput Aided Mol Des. 2010 Apr; 24(4):317–333.

[25] **Klamt A**, Diedenhofen M, Some conclusions regarding the predictions of tautomeric equilibria in solution based on the SAMPL2 challenge; 2010.

[26] **Marenich AV**, Ho J, Coote ML, Cramer CJ, Truhlar DG. Computational electrochemistry: prediction of liquid-phase reduction potentials. Phys Chem Chem Phys. 2014; 16(29):15068–15106.

[27] **Irikura KK**, Frurip DJ. Computational Thermochemistry: Prediction and Estimation of Molecular Thermodynamics. Amer Chemical Society; 1998.

[28] **Zhou HX**, Gilson MK, Theory of Free Energy and Entropy in Noncovalent Binding; 2009.

[29] **Lin CY**, Izgorodina EI, Coote ML, How Accurate Are Approximate Methods for Evaluating Partition Functions for Hindered Internal Rotations?; 2008.

[30] **Head MS**, Given JA, Gilson MK, "Mining Minima": Direct Computation of Conformational Free Energy; 1997.

[31] **Chang CEA**, Chen W, Gilson MK. Ligand configurational entropy and protein binding. Proceedings of the National Academy of Sciences. 2007 Jan; 104(5):1534–1539.

[32] **Smith JS**, Isayev O, Roitberg AE, ANI-1: an extensible neural network potential with DFT accuracy at force field computational cost; 2017.

[33] **Unke OT**, Meuwly M, PhysNet: A Neural Network for Predicting Energies, Forces, Dipole Moments, and Partial Charges; 2019.

[34] **Schütt KT**, Sauceda HE, Kindermans PJ, Tkatchenko A, Müller KR, SchNet – A deep learning architecture for molecules and materials; 2018.

[35] **Dral PO**, Quantum Chemistry in the Age of Machine Learning; 2020.

[36] **Becke AD**. Density-functional exchange-energy approximation with correct asymptotic behavior. Physical Review A. 1988 sep; 38(6):3098–3100. https://link.aps.org/doi/10.1103/PhysRevA.38.3098, doi: 10.1103/PhysRevA.38.3098.

[37] **Lee C**, Yang W, Parr RG. Development of the Colle-Salvetti correlation-energy formula into a functional of the electron density. Physical Review B. 1988 jan; 37(2):785–789. https://link.aps.org/doi/10.1103/PhysRevB.37.785, doi: 10.1103/PhysRevB.37.785.

[38] **Kendall RA**, Dunning TH, Harrison RJ. Electron affinities of the first-row atoms revisited. Systematic basis sets and wave functions. The Journal of Chemical Physics. 1992; 96(9):6796–6806. doi: 10.1063/1.462569.

[39] **Hehre WJ**, Ditchfield R, Pople JA. Self — Consistent Molecular Orbital Methods . XII . Further Extensions of Gaussian — Type Basis Sets for Use in Molecular Orbital Studies of Organic Molecules Published by the AIP Publishing Articles you may be interested in Self - consistent molecular or. JChem Phys. 1972; 56(5):2257–2261.

[40] **Francl MM**, Pietro WJ, Hehre WJ, Binkley JS, Gordon MS, DeFrees DJ, Pople JA. Self-consistent molecular orbital methods. XXIII. A polarization-type basis set for second-row elements. The Journal of Chemical Physics. 1982; 77(7):3654–3665. doi: 10.1063/1.444267.

[41] **Marenich AV**, Cramer CJ, Truhlar DG. Universal Solvation Model Based on Solute Electron Density and on a Continuum Model of the Solvent Defined by the Bulk Dielectric Constant and Atomic Surface Tensions. J Phys Chem B. 2009 May; 113(18):6378–6396.

[42] **Soteras I**, Orozco M, Javier Luque F, Performance of the IEF-MST solvation continuum model in the SAMPL2 blind test prediction of hydration and tautomerization free energies; 2010.

[43] **Elguero J**. Tautomerism. In: *Brenner's Encyclopedia of Genetics* Elsevier; 2013.p. 18–22.

[44] **Kenny P**. The Prediction of Tautomer Preference in Aqueous Solution (Version 1.0). . 2019 Jul; .

[45] **Nicholls A**, Wlodek S, Grant JA. The SAMP1 Solvation Challenge: Further Lessons Regarding the Pitfalls of Parametrization †. J Phys Chem B. 2009 Apr; 113(14):4521–4532.

[46] **Schlund S**, Basílio Janke EM, Weisz K, Engels B. Predicting the tautomeric equilibrium of acetylacetone in solution. I. The right answer for the wrong reason? Journal of Computational Chemistry. 2009; 30(10):NA–NA. http://doi.wiley.com/10.1002/jcc.21354, doi: 10.1002/jcc.21354.

[47] **Neal RM**. Annealed Importance Sampling. . 1998; (9805):1–25.

[48] **Ebejer JP**, Morris GM, Deane CM, Freely Available Conformer Generation Methods: How Good Are They?; 2012.

[49] **Havel TF**, Distance Geometry: Theory, Algorithms, and Chemical Applications; 2002.

[50] **Neese F**, The ORCA program system; 2012.

[51] **Grimme S**, Antony J, Ehrlich S, Krieg H. A consistent and accurate ab initio parametrization of density functional dispersion correction (DFT-D) for the 94 elements H-Pu. Journal of Chemical Physics. 2010; 132(15). doi: 10.1063/1.3382344.

[52] **Grimme S**, Supramolecular Binding Thermodynamics by Dispersion-Corrected Density Functional Theory; 2012.

[53] Jmol: an open-source Java viewer for chemical structures in 3D;. Accessed: 2020-10-10. http://www.jmol.org/.

[54] **Ho J**, Ertem MZ, Calculating Free Energy Changes in Continuum Solvation Models; 2016.

[55] **Parrish RM**, Burns LA, Smith DGA, Simmonett AC, Eugene DePrince A, Hohenstein EG, Bozkaya U, Sokolov AY, Di Remigio R, Richard RM, Gonthier JF, James AM, McAlexander HR, Kumar A, Saitow M, Wang X, Pritchard BP, Verma P, Schaefer HF, Patkowski K, et al., Psi4 1.1: An Open-Source Electronic Structure Program Emphasizing Automation, Advanced Libraries, and Interoperability; 2017.

[56] **Larsen AH**, Mortensen JJ, Blomqvist J, Castelli IE, Christensen R, Dułak M, Friis J, Groves MN, Hammer B, Hargus C, Hermes ED, Jennings PC, Jensen PB, Kermode J, Kitchin JR, Kolsbjerg EL, Kubal J, Kaasbjerg K, Lysgaard S, Maronsson JB, et al., The atomic simulation environment—a Python library for working with atoms; 2017.

[57] **Leimkuhler B**, Matthews C. Molecular Dynamics: With Deterministic and Stochastic Numerical Methods. Springer; 2015.

[58] **Shirts MR**, Chodera JD. Statistically optimal analysis of samples from multiple equilibrium states. J Chem Phys. 2008 Sep; 129(12):124105.

Detailed methods

Experimental data

The full dataset considered for this study was obtained from the DataWarrior File deposited in https://github.com/WahlOya/Tautobase (commit of Jul 23, 2019), described in detail in [12]. The dataset was sourced from the tautomer codex authored by P.W. Kenny and P.J. Taylor [44].

From the dataset a subset of tautomer pairs were considered that

1. were measured/calculated/estimated in aqueous solution
2. had a logK value between +/-10
3. had a numeric logK value
4. had no charged species
5. did not contain iodine
6. only a single hydrogen changed its position

476 of the 1680 deposited tautomer pairs had these properties. We added two tautomer pairs from the SAMPL2 challenge (Tautomer pair 2A_2B and 4A_4B) [21]. 478 unique tautomer pairs were considered for further analysis. Unique tautomer pairs means that the combination of the two tautomers has to be unique, not the individual molecule. In the following we will use an identifier containing the row number entry from the original DataWarrier file to identify molecules in the dataset, e.g. molDWRow_200 describing the tautomer pair at row number 200 in the original DataWarrior file.

The logK value was converted to free energy differences with $\Delta G^{exp}_{solv} = -RT \ln K$. The free energy difference of the tautomer pairs obtained from the Tautobase are subsequently referenced as ΔG^{exp}_{solv} in contrast to the calculated values which are called ΔG^{calc}. While we call all values deposited in the Tautobase G^{exp}_{solv} we want to point out that some of these values are estimated or calculated.

A closer inspection of some of the outliers identified incorrectly drawn structures in the database (Row entry: 1260,1261,1262,1263,1264,514,515,516,517,1587) – these 10 tautomer pairs were subsequently removed from all further analysis. Removing these 10 tautomer pairs resulted in 468 tautomer pairs. Additionally, 8 tautomer pairs (Row entry: 989, 581, 582, 617, 618, 83, 952, 988) were removed from calculations performed with the basis set 6-31G(d) dataset containing bromide since there are no parameters available.

For calculations that involved ANI we had to remove tautomer pairs from the dataset that contained elements not included in the ANI training set (only C,N,H,O) resulting in 369 tautomer pairs. Furthermore, all molecules with a stereobond that changed its position in both tautomers were removed (this affected 15 tautomer pairs: molDWRow_1637, molDWRow_510, molDWRow_513, molDWRow_515, molDWRow_517, molDWRow_518, molDWRow_787, molDWRow_788, molDWRow_789, molDWRow_810, molDWRow_811, molDWRow_812, molDWRow_865, molDWRow_866, molDWRow_867).

The subset of the Tautobase used for the QM calculations can be obtained here as list of SMILES (468 tautomer pairs): https://github.com/choderalab/neutromeratio/blob/master/data/b3lyp_tautobase_subset.txt. The subset of the Tautobase used for the QML calculations can be found here as list of SMILES (354 tautomer pairs): https://github.com/choderalab/neutromeratio/blob/master/data/ani_tautobase_subset.txt. The distribution of the experimental solvation free energies for both datasets are shown in 11.

Generating molecular conformations

The input tautomer pairs were specified as SMILES strings. 3D conformations were generated with the chemoinformatics toolkit RDKit (version 2019.09.2) which uses the distance geometry approach to generate conformations while enforcing chirality/stereochemistry [48, 49] For each molecule 20 conformations were initially generated. The number of conformations was reduced to 10 if the average root mean square deviation (RMSD) of atoms of the 20 conformations was below 0.5 Angstrom, and further reduced to 5 conformations if below 0.2 Angstrom.

RMSD calculations and filtering of conformations

For each molecule, pairwise RMSD between conformations were calculated using RDKit. Starting with a random conformation, if the RMSD to any other conformation of the molecule was below 0.1 the con-

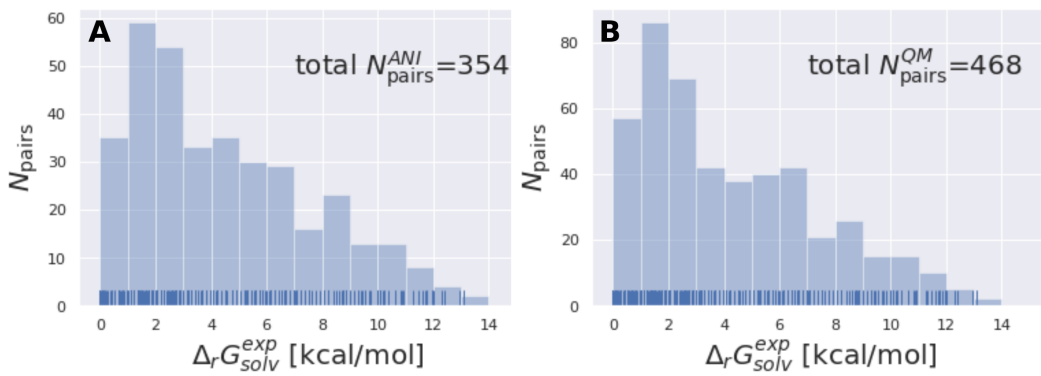

Appendix 0 Figure 11. The tautomer dataset shows a wide variety of solvation free energies ΔG_{solv}^{exp}. A shows the ANI-Tautobase subset that was used for the QML calculations and B shows the QM-Tautobase subset used for the QM calculations. The full dataset considered for this study was obtained from the DataWorrier File deposited at https://github.com/WahlOya/Tautobase (commit of Jul 23, 2019), described in detail in [12]. The selection criteria for both datasets are described in detail in Detailed methods section.

formation is discarded, otherwise added to the list of unique conformations. The RMSD was calculated between heavy atoms and the hydrogen of selected chemical moieties including primary alcohols, imines, primary/secondary amines, cyanamides and thiols.

Quantum mechanical calculations

Orca and continuum solvation models for tautomer reaction free energy calculations in solution

Quantum mechanical calculations were performed using the quantum chemical software orca 4.0.1.2 [50].

Geometric optimization was performed with the standard options of orca, redundant internal coordinates and the BFGS optimizer using B3LYP/aug-cc-pVTZ [36–38] in vacuum and with a continuum solvation model. The universal solvation model based on solute electron density (SMD) was used as continuum solvation model [41].

Frequency calculations were performed with the numerical Hessian computed using the central differences approach. If a conformation had negative frequencies (imaginary modes) after the geometry optimization it was excluded from further analysis. Single point calculations were performed on the optimized geometries using B3LYP/aug-cc-pVTZ and B3LYP/6-31G(d) [39, 40] in vacuum and in the continuum solvation model. A damping dispersion correction was applied (orca keyword D3BJ) [51].

Thermal corrections were computed at standard state (298.15 K and 1 atm pressure) using the ideal gas molecular partition function and the rigid-rotor harmonic oscillator (RRHO) approximation. Since there is a volume change in the standard state from the gas phase (1 atm) to the solvent phase we indicate each phase either with '*' (gas phase standard state) or with '∘' (solution standard state). Low-lying vibrational frequencies (below 15 cm-1) were treated by a free-rotor approximation [52] – this method is also sometimes called rigid-rotor quasi harmonic oscillator.

The rotational symmetry number was obtained from the point group of the tautomer using the point group module of Jmol and visual inspection [53].

The Gibbs free energy $G_{gas,k}^{*}$ was then obtained by adding thermal corrections $G_{T,k}^{*}$ (and $\epsilon_{ZPE,K}$) to the electronic energy E_k for a given coordinate set (k).

$$G_{gas,k}^{*} = E_k + \epsilon_{ZPE,k} + G_{T,k}^{*} - RT \ln D \tag{6}$$

The degeneracy D was estimated by calculating the graph automorphism of the molecule. The implementation of the VF2 algorithm for graph isomorphism of networkx (https://networkx.github.io/documentation/stable/citing.html) was used. Nodes were defined to match if element and hybridization matched, edges were identical if bond order matched.

SMD is used to model the molecules in aqueous environment. The standard-state free energy of solvation is then defined as

$$\Delta G_S^\circ = \Delta G^{*\to\circ} + \Delta G_{ENP} + G_{CDS} \tag{7}$$

with $\Delta G^{*\to\circ}$ as standard-state adjustments (specifically, the correction of changing the volume from the gas phase to the solute phase with a constant value of 1.89 kcal/mol), ΔG_{ENP} describes the electronic (E), nuclear (N) and polarization (P) components of the free energy and Δ_{CDS} free energy changes associated with solvent cavitation (C), changes in dispersion (D) and changes in local solvent structure (S) [41]. The reaction free energy was computed as the difference in the free energies of both tautomer species.

Another possible way to calculate a reaction free energy in solution is to carry out the electronic structure calculation in the continuum solvation reaction field and using the ideal gas molecular partition function in combination with the RRHO approximation to obtain solution phase free energies. The free energy in solution is calculated using

$$G_{aq,k}^\circ = \left\langle \psi^{sol} | H^g + \frac{V}{2} | \psi^{sol} \right\rangle + G_{NES} + G_{T,K} \tag{8}$$

where ψ^{sol} is the polarized wave function in solution, H^g the gas phase Hamiltonian, and V the potential energy operator associated with the reaction field. The bracket term describes the electronic energy, while G_{NES} is associated with non-electrostatic contributions (dispersion-repulsion and solvent structural terms) to the solvation energy and $G_{T,K}$ are the thermal correction calculated directly in the continuum solvation model [54].

We calculated the solvation free energy ΔG_{solv}^{calc} for 468 tautomer pairs using three approaches. Generating multiple conformations, optimizing with B3LYP/aug-cc-pVTZ in gas phase and solution phase (using the SMD solvation model) and calculating ΔG_{solv}^{calc} as the sum of the gas phase free energy (evaluated on the gas phase conformation) and the difference between the single point energy in gas phase (gas phase conformations) and solvent (solvent phase conformation) calculated on the B3LYP/aug-cc-pVTZ level of theory. The individual $\Delta G_{solv,k}^{calc}$ for conformation k are then Boltzmann averaged to obtain the final ΔG_{solv}^{calc}.

Generating multiple conformations, optimizing with B3LYP/aug-cc-pVTZ in gas phase and solution phase (using the SMD solvation model) and calculating ΔG_{solv}^{calc} as the sum of the gas phase free energy (evaluated on the gas phase conformation) and the difference between the total energy in gas phase (evaluated on the gas phase conformation) and solvent phase (evaluated on the solvent phase conformation) on the B3LYP/6-31G level of theory. The individual $\Delta G_{solv,k}^{calc}$ for conformation k are then Boltzmann averaged to obtain the final ΔG_{solv}^{calc}.

Generating multiple conformations, optimizing with B3LYP/aug-cc-pVTZ in solution phase (using the SMD solvation model) and calculating ΔG_{solv}^{calc} directly as the difference between the IG-RRHO free energy calculated in solution (and on the solution phase geometry). The individual $\Delta G_{solv,k}^{calc}$ for conformation k are then Boltzmann averaged to obtain the final ΔG_{solv}^{calc}.

Single point energy calculations with psi4

The electronic structure calculation was performed using the $\omega B97X$ density functional and the 6-31G(d) basis set with the quantum chemical program psi4 [55]. Geometric optimization was performed using redundant internal coordinates and BFGS Hessian updates. Using the optimized geometry electronic structure calculations were performed with machine learning potential ANI1x [32] as implemented in torchANI.

ASE thermochemistry corrections

For each molecule 100 conformations were generated. ANI1ccx was used to calculate the electronic energy. The conformations were minimized using the BFGS optimizer as implemented in scipy. Frequency and thermochemistry calculations were performed using the optimized geometry. Thermal corrections were calculated for 298 K and 1 atm using the IG-RRHO approximation as implemented in the atomic simulation environment (ase) [56]. ΔG_{vac} was then calculated as the difference between G_{gas}° of the tautomer pair.

Relative alchemical free energy calculations

Relative alchemical free energies were calculated using a single, hybrid topology approach for gas phase and solvation phase. The topology of each tautomer pair only differed in the position of a single hydrogen (bonds and bonded types were not specified). The hybrid topology (the superset of the two topologies) differed therefore by one hydrogen from each of the physical endstates.

As default, the coordinates of the hybrid topology were generated by using the coordinates of tautomer 1 (as defined in the initial tautomer database). If a tautomer isomerismn created or removed a cis/trans stereobond, the initial coordinates were taken from the topology with the stereobond present (therefore sometimes changing the direction of the tautomer reaction).

The coordinates of the added, non-interacting hydrogen were obtained by randomly sampling 100 hydrogen positions around its new bonded heavy atom and subsequently using the lowest energy position. The physical endstates (representing the two tautomer states, each with an additional non-interacting (dummy) hydrogen) were connected via 11 intermediate (lambda) states.

Energy and forces were calculated using ANI1ccx and ANI1x as implemented in torchani https://github.com/aiqm/torchani). The energy as well as the resulting force was linearly scaled along the alchemical path as a function of lambda with

$$E = (1 - \lambda)E_1 + \lambda E_2 \tag{9}$$

Before each simulation, initial coordinates were minimized using BFGS optimizer as implemented in scipy. Coordinates were sampled using Langevin dynamics at 300 K with a collision rate of 10 ps^{-1} and a 0.5 fs time step using the BAOAB integrator [57]. Initial velocities were obtained from a Maxwell-Boltzmann distribution at the simulation temperature.

200 ps simuation time was used to obtain smaples from each lambda state Simulation The gas phase simulations were repeated 5 times with randomly seeded initial velocities (and coordinates).

All bonds involving hydrogens were restrained throughout the simulation at each lambda states using a flat bottom potential well with harmonic walls. The restraint was defined as

$$E = H(\Delta(r_{i,j}, r^0_{i,j}) - r_{fb}) * \frac{k_{i,j}}{2}(\Delta(r_{i,j}, r^0_{i,j}) - r_{fb})^2 \tag{10}$$

with H as the Heaviside step function, $\Delta(r_{i,j}, r^0_{i,j})$ as the difference between the reference bond length $r^0_{i,j}$ and the current bond length $r_{i,j}$ and r_{fb} as half of the well radius. For all heavy atom pairs $r^0_{i,j}$ was set to 1.3 Angstrom and r_{fb} to 0.3 Angstrom. For C-H/O-H/N-H bond pairs $r^0_{i,j}$ was set to 1.09/0.96/1.01 Angstrom and r_{fb} to 0.4 Angstrom.

Alchemical free energy differences in vacuum ΔG^{calc}_{vac} were calculated using MBAR as implemented in the pymbar package [58]. To remove correlated snapshots from the MBAR analysis the time series functions of pymbar were used to detect the equilibrated region of the trajectory. 300 uncorrelated snapshots were considered for the MBAR analysis for each lambda state.

Neural net parameter optimization based on experimental free energy differences

The tautomer data set was split into a test set (71 tautomer pairs), validation set (57 tautomer pairs) and training set (226 tautomer pairs). Gradient updates were performed on the training set, the best model was validated based on the RMSE on the validation set and used to evaluate the model performance on the test set.

Neural net parameters were optimized using a routine modified from the TorchANI tutorial[1]. To limit the capacity to overfit, only the weights and biases of the *final* layer of each of the 8 pretrained ANI-1ccx models were optimized for each of the atom nets (one net per element). As in the TorchANI tutorial, the weight matrices were updated using the Adam optimizer with decoupled weight decay, and the bias vectors were updated using Stochastic Gradient Descent (SGD). The weight decay rate was set to 10^{-6}.

[1] https://aiqm.github.io/torchani/examples/nnp_training.html

The model was trained by minimizing the MSE loss between calculated and experimental free energies. The per molecule pair (m) loss function l is defined as

$$l(m;\theta) = \left(\Delta G^{exp}_{solv,m} - \Delta G(\theta)^{calc}_{vac,m}\right)^2 \tag{11}$$

with $\Delta G^{exp}_{solv,m}$ as the experimental and $\Delta G(\theta)^{calc}_{vac,m}$ as the calculated reaction free energy value for molecule m at parameters θ. $\Delta G^{calc}_{solv,m}$ is a function of the individual energies per lambda state, which are a function of the input parameters θ and the coordinate set. The overall loss is then

$$L(\theta) = \sum_m l(m;\theta) \tag{12}$$

.

The perturbed free energy $\Delta G(\theta)^{calc}_{vac,m}$ required for computing $l(m;\theta)$ is calculated by importance sampling, or "reweighting" the original MBAR estimate from the original pre-trained parameters θ^* to the current parameters θ. To compute this estimate efficiently at arbitrary θ, we first collect configuration samples at a reference value θ^* (corresponding to the original parameters of the pretrained ANI-1ccx model) for each intermediate value λ. For each configuration sample x, we compute the reduced potential $u(x, \lambda; \theta^*)$, to form the $N \times M$ matrix of inputs to MBAR. (Where N is the total number of snapshots, M is number of λ windows.) MBAR equations are solved to yield a vector of reduced free energies f^*_m, where m indexes the intermediate λ values. The reaction free energy prediction implied by the model parameters θ^* is then $f^*_M - f^*_1$.

To compute reaction free energy at a new value of the parameters θ, we need to compute $u(x, \lambda = 1; \theta)$ and $u(x, \lambda = 0; \theta)$ for all configurations x. The optimization routine evaluates the gradient of the loss function L w.r.t. θ by automatic differentiation and updates the parameters.

300 uncorrelated snapshots per λ state were used for the MBAR estimate and importance sampling for the vacuum simulations.

name		ΔG_{solv}^{exp}	ΔG_{solv}^{calc}
molDWRow_1668	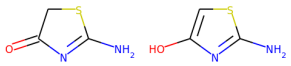	5.5	15.9
molDWRow_1669	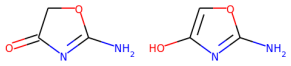	9.5	21.5
molDWRow_1670	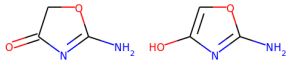	6.8	17.6
molDWRow_1559	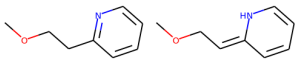	2.7	18.9
molDWRow_331	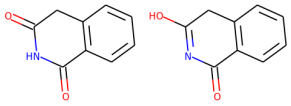	2.2	12.8
molDWRow_853	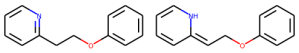	1.4	18.6

Appendix 0 Table S.I.1. 5 out of the 6 tautomer pairs with the highest absolute error have common scaffolds. Tautomer pairs with absolute errors above 10 kcal/mol are shown.

Supplementary Information

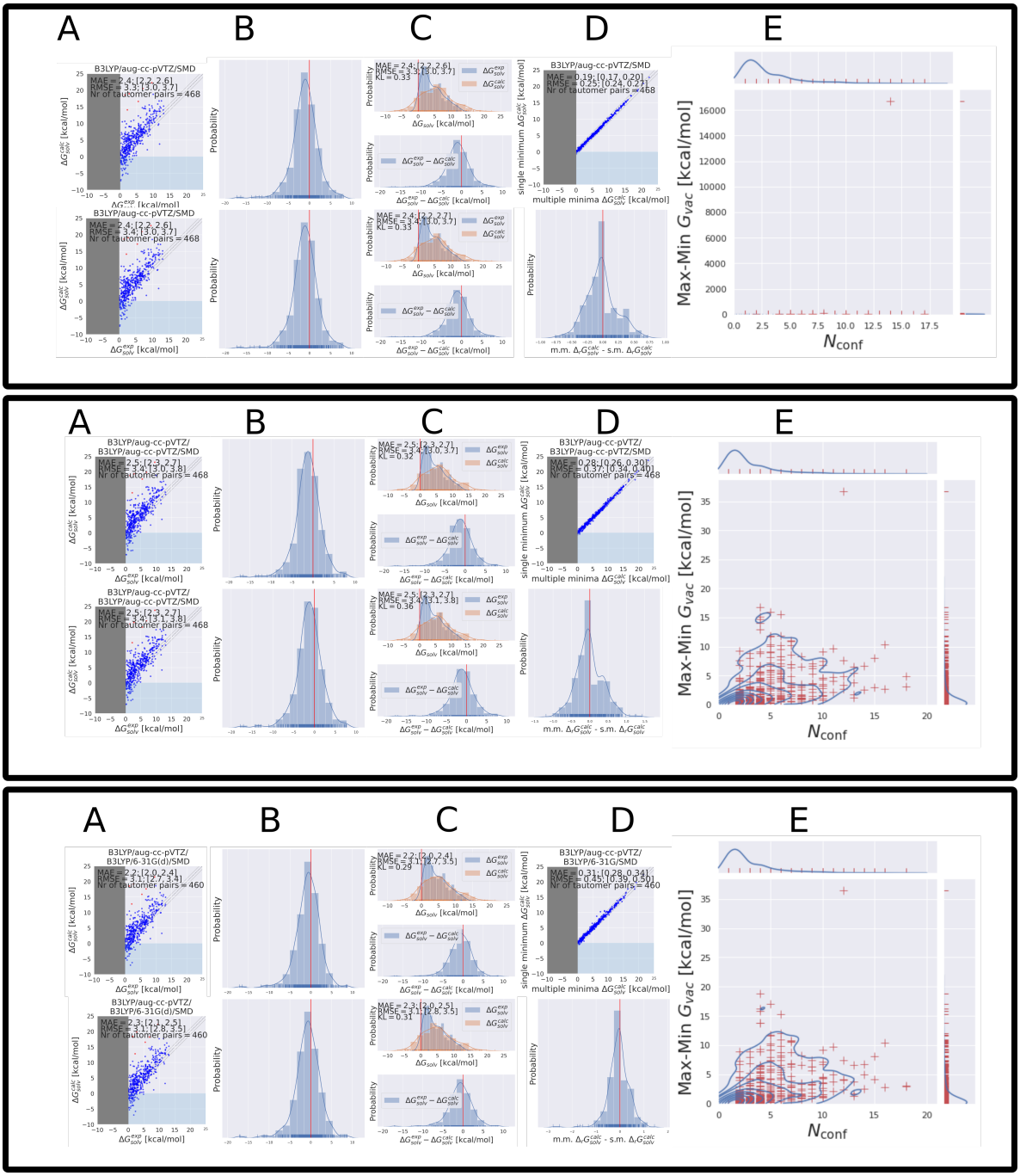

Appendix 0 Figure S.I.1. Each of the three blocks show the QM calculations done with different level of theory indicated by the title in the plots in column A. In each block the top penal shows the results obtained with multiple minimum conformations, the bottom penal shows the results obtain with a single conformation. Column **D** shows the difference between the multiple minimum and single minimum approach and **E** show the the number of minimum conformations against the difference between the lowest and highest energy for each tautomer. These results were obtained without the additional structure symmetry correction.

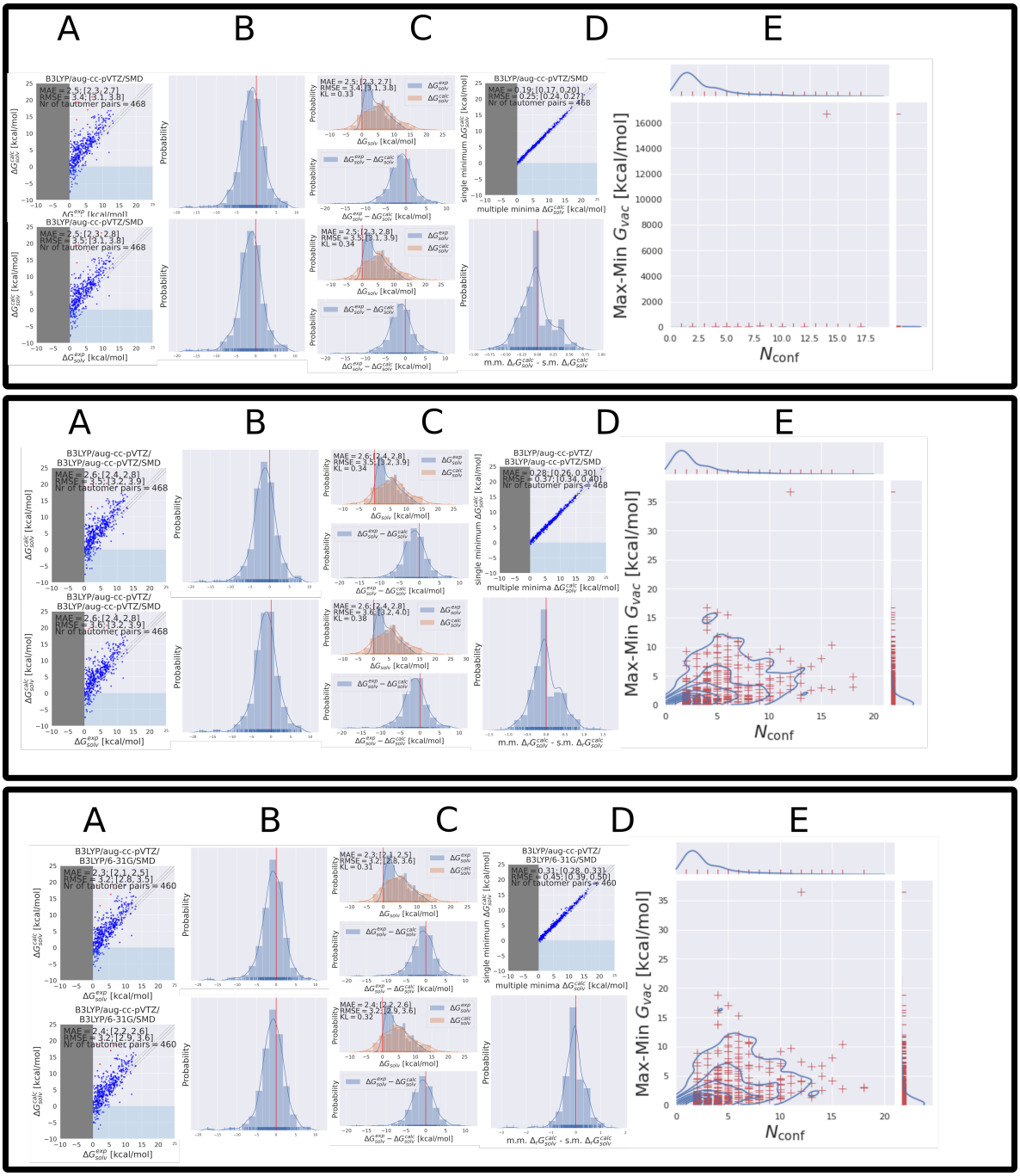

Appendix 0 Figure S.I.2. Each of the three blocks show the QM calculations done with different level of theory indicated by the title in the plots in column A. In each block the top penal shows the results obtained with multiple minimum conformations, the bottom penal shows the results obtain with a single conformation. Column **D** shows the difference between the multiple minimum and single minimum approach and **E** show the the number of minimum conformations against the difference between the lowest and highest energy for each tautomer. These results were obtained **with** structure symmetry correction.